ASSESSMENT OF FLOW-INDUCED STRESSES IN PIPES WITH BENDS

SHAHAB AHMADIZADE[1], SUYASH VERMA[1], MUHAMMAD SAIF ULLAH KHALID[1,2] AND ARMAN HEMMATI[1]

[1]Department of Mechanical Engineering, University of Alberta, Edmonton, AB, T6G 2R3, Canada
arman-hemmati@ualberta.ca
[2]Department of Mechanical and Mechatronics Engineering, Lakehead University, Thunder Bay, ON, P7B 5E1 Canada
mkhalid7@lakeheadu.ca

Key words: CFD, FSI, OpenFoam, Solids4foam, Pipeline.

Abstract. This study numerically investigates flow-induced stresses and displacements in bent pipes at varying angles ($20^\circ \leq \theta_b \leq 80^\circ$) using Solids4Foam at Reynolds number of 20,000. The results indicate that increasing θ_b enhances the formation of symmetric vortex structures, which coincide with enhanced non-uniformity in pressure distribution and wall shear stresses. Additionally, maximum equivalent stresses (σ_{eq}) for the solid shell occur near the inlet. The pipes with higher θ_b also depict a reduced displacement magnitude($\boldsymbol{D}$), which hints at the strong role of fixed displacement boundary condition assigned at the pipe inlet and outlet. These findings provide essential insights for performing numerical investigation of pipeline reliability and structural integrity in oil transportation.

1 INTRODUCTION

Fluid-structure interaction (FSI) is a critical area of research that focus on the coupling between fluid and structural dynamics. This interaction plays a vital role in engineering applications across industries, including aerospace, biomechanics, civil engineering, and marine engineering [1]. In pipelines, understanding FSI phenomena is particularly crucial, as flow-induced vibrations can lead to potential failures, compromising operational efficiency and safety [2]. Accurate simulation and comprehensive analysis of FSI are essential for optimizing design operation of pipelines to ensure reliability and structural integrity. Neglecting these interactions can result in catastrophic consequences [3]. For these reasons, studying pipe flows, especially flows in bent pipes, is of interest to researchers, leading to numerous experimental and numerical studies. Fluid dynamics in bend pipes exhibit complex phenomena, such as Dean motion and swirl switching motion, that can significantly alter the flow characteristics downstream of the bend [4, 5]. Dean motion, characterized by secondary flow patterns, is induced by centrifugal forces acting in the flow. This creates a pair of counter-rotating vortices that can intensify turbulence and disrupt flow distribution downstream [5].

Spedding et al. [8] suggested that flow through 90° bends is characterized by complex secondary flow patterns and significant pressure drops that are influenced by factors such as Reynols number and bend geometry. These factors can be investigated in order to optimize industrial piping systems. The experimental study of Sudo et al. [6] highlighted that turbulent flow in both square-sectioned 90° bends and circular-sectioned 180° bends [7], generate complex secondary flows and significant turbulence intensity variation. Moreover, the flow structure was highly dependent on Reynolds number and bend geometry. Vaghefi et al. [9] also examined the mean and turbulent flow sharp open channel bend 180° that highlight the significant effects of secondary flow on shear stress distribution along the bend. Yarahmadi [10] examined a 90° bend, studying shear stress behavior. Crawford and Spence [11] numerically investigated turbulent flow in 90° elbow bends that uncovered detailed flow structures and quantified energy losses, highlighting the impact of elbow geometry on flow efficiency. Thus, they provided guidance for improved bend design in engineering applications [11]. With respect to FSI analysis, Miwa et al. [12] investigated two-phase flow-induced vibrations in piping systems for straight pipes. This study offered insights into vibration mechanisms and their implications for the design and safety of nuclear energy systems. Pontaza et al. [13] further conducted a numerical study on high gas rate well jumpers, which highlighted significant differences in vibration characteristics and structural impacts between configurations with tees and bends. This finding can improve subsea design pipelines [13].

Previous studies have extensively explored the flow physics in bend pipes, particularly focused on development of secondary flow patterns, such as Dean motion [4, 5]. These investigations have provided valuable insights into velocity profiles, pressure gradients, and turbulence characteristics within curved sections. However, there remains a significant gap in the literature regarding a comprehensive analysis of FSI in bend pipes with varying θ_b. This study, therefore, aims to address this gap by investigating the flow-induced stresses and displacements for bend pipes at a wider range of θ_b.

2 PROBLEM DESCRIPTION & METHODOLOGY

This numerical study models FSI in pipes with varying θ_b in the range $20^\circ \leq \theta_b \leq 80^\circ$ at Reynolds number of 20,000. The pipe bend radius is r = 2D and wall thickness is 0.0135D, where D represents the pipe diameter (see Figure 1). The structural behavior was simulated using a linear elastic model, based on API X70 steel properties. Fluid and solid properties are summarized in Tables 1 and 2, respectively.

Solids4Foam [14] numerical solver within OpenFOAM [15] is utilized for this analysis, which employs a monolithic method for two-way coupled FSI simulations. This solver enables accurate FSI modeling by solving both Navier-Stokes and structural equations simultaneously, ensuring a strong coupling between the solid and fluid domains. For the fluid region, a fully developed velocity profile was specified at the inlet boundary, while a zero pressure gradient was applied at the outlet. A no-slip boundary condition was enforced at the walls to accurately simulate the flow characteristics. With respect to the solid pipe shell, a fixed displacement boundary condition was applied at both ends of the pipe, while a free traction was applied on

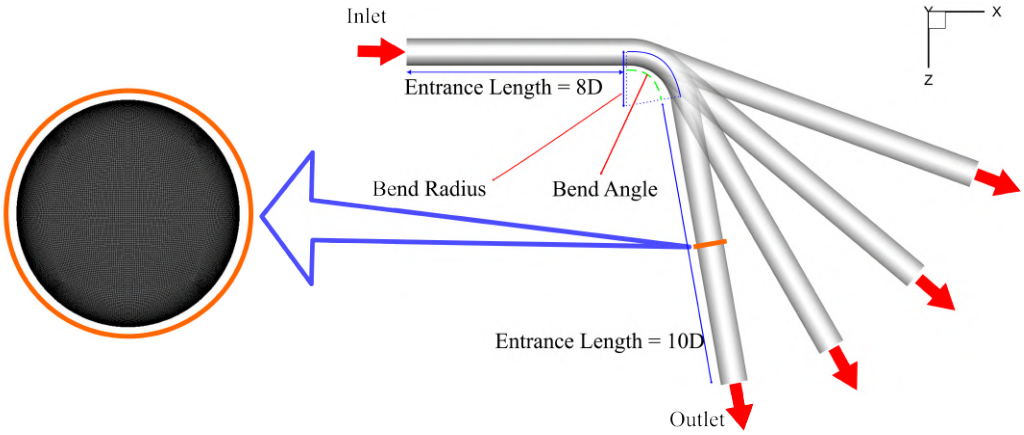

Figure 1: Dimension and parameters of computational domain and a sectional view of the fluid mesh.

the outer and inner wall of the solid shell. Hexahedral structured mesh with a total of 7×10^6 and 0.6×10^6 elements was employed for fluid and solid regions, respectively. A section of the fluid mesh is depicted in Figure 1.

The pimpleFoam solver was utilized to couple velocity and pressure fields for the fluid domain, which is suitable for incompressible, transient flows. k-ω Reynolds-averaged Navier–Stokes turbulence model was implemented due to its robustness in dealing with boundary layer flows under adverse pressure gradients. For the solid domain, LinearGeometry model was used to solve the governing equations, leveraging its capability to handle linear elastic behavior accu-

Table 1: Flow Properties

Property	**Value**
Mean Velocity (U_b)	0.413 m/s
Kinematic Viscosity (ν)	1.55078×10^{-5} m²/s
Reynolds Number (Re)	20000

Table 2: Solid Properties

Property	**Value**
Material	API X70 Steel
Density (ρ_s)	7860 kg/m³
Young's Modulus (E)	210 GPa
Poisson's Ratio (ν_s)	0.3

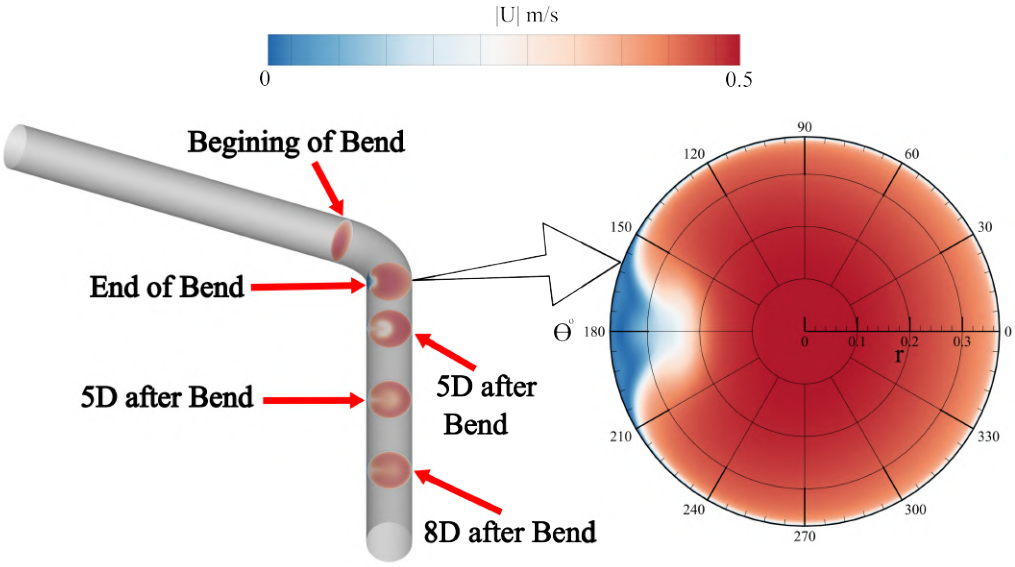

Figure 2: Locations employed for data extraction along the flow directions.

rately [14]. This model is appropriate for simulating the structural response of pipes made from API X70 steel. For the FSI analysis, Aitken relaxation method was employed, which enhances the convergence stability by iteratively adjusting the relaxation factor based on the convergence history [14]. The General Grid Interface (GGI) method facilitated data transfer between the fluid and solid domains.

3 RESULTS AND DISCUSSIONS

We begin by investigating the flow behavior across different fluid sections, followed by a brief discussion on the distribution of equivalent stress (σ_{eq}) and displacement magnitude ($\boldsymbol{D}$) along the solid shell region of the pipe. For brevity, the observations are only discussed for θ_b corresponding to 20°, 40°, 60° and 80°.

Figure 2 provides qualitative visualization of the velocity magnitude ($|U|$) at different locations along the pipe that helps in evaluating the flow behavior along the circumference of the pipe. Note that the azimuthal coordinate in Figure 2 is denoted by θ. The selection of locations is, primarily, governed by the onset of flow separation and re-circulation observed ahead of the bend inlet. In order to compare the changes in the most critical aspects of the flow behavior across different θ_b, we further choose to present the findings only at two selective locations. These include the bend outlet (Figure 3(a-d)), and 8D downstream of the bend (Figure 3(e-h)), respectively. We observe that increasing θ_b enhances the effect of symmetric vortices at the end of the bend. This effect is qualitatively characterized in terms of the growth of velocity deficit regions at $\theta = 180°$. However, contours at 8D downstream of the bend depict a reduction in the recovery length required for dampening these vortices as θ_b increases from 20° to 80°. The apparent fluid flow patterns contributes to a non-uniform distribution of flow induced pressure(p)

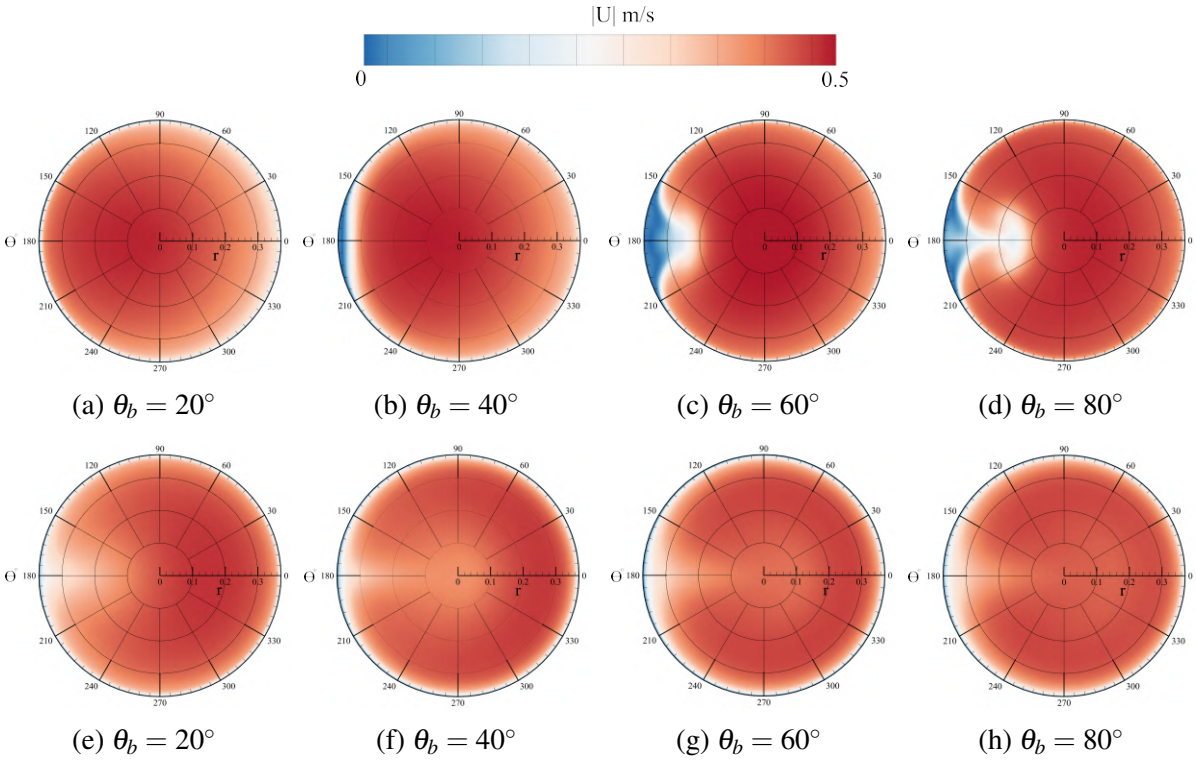

(a) $\theta_b = 20°$ (b) $\theta_b = 40°$ (c) $\theta_b = 60°$ (d) $\theta_b = 80°$

(e) $\theta_b = 20°$ (f) $\theta_b = 40°$ (g) $\theta_b = 60°$ (h) $\theta_b = 80°$

Figure 3: Contours representing $|U|$ at the bend outlet, (a-d) and 8D after bend outlet (e-h), for pipes at increasing θ_b.

and shear stress (τ_w) along the pipe wall.

Figure 4(a) depicts the distribution of p/p_o corresponding to $\theta_b = 80°$. Here, p_o represents the dynamic pressure expressed as $0.5\rho U_b^2$. The region along the bend at $90° \leq \theta \leq 270°$ depicts a pressure drop that coincides with the growth of velocity deficit region, as confirmed at the bend outlet in Figure 3(d). Contrarily, an intensification of τ_w is apparent within the same region (see Figure 4(b)). As θ_b decreases towards 20°, the spatial non-uniformity of p/p_o undergoes a decrease along the bend region at $90° \leq \theta \leq 270°$. The qualitative observations for $\theta_b < 80°$ are not shown here for brevity. A similar decrease in spatial non-uniformity and magnitude is also apparent for τ_w, as θ_b decrease towards 20°. The changes in p/p_o and τ_w along the circumference of the pipe wall are associated with the existence of secondary vortices in the flow within the bend and downstream of bend outlet [5]. As the Dean and swirl motion damped with decreasing θ_b, the velocity deficit region shrunk (noticed in Figure 3), which inherently led to a symmetric distribution of p/p_o and τ_w in the bend section and downstream areas.

The behavior of $\boldsymbol{D}$ and σ_{eq} is in contrast to the observations discussed for p/p_o and τ_w in the fluid region. Particularly, the maximum of $\boldsymbol{D}$ (see Figure 5(a)) and σ_{eq} (see Figure 5(b)) is observed for the pipe bend corresponding to $\theta_b = 20°$. We observe that the maximum $\boldsymbol{D}$

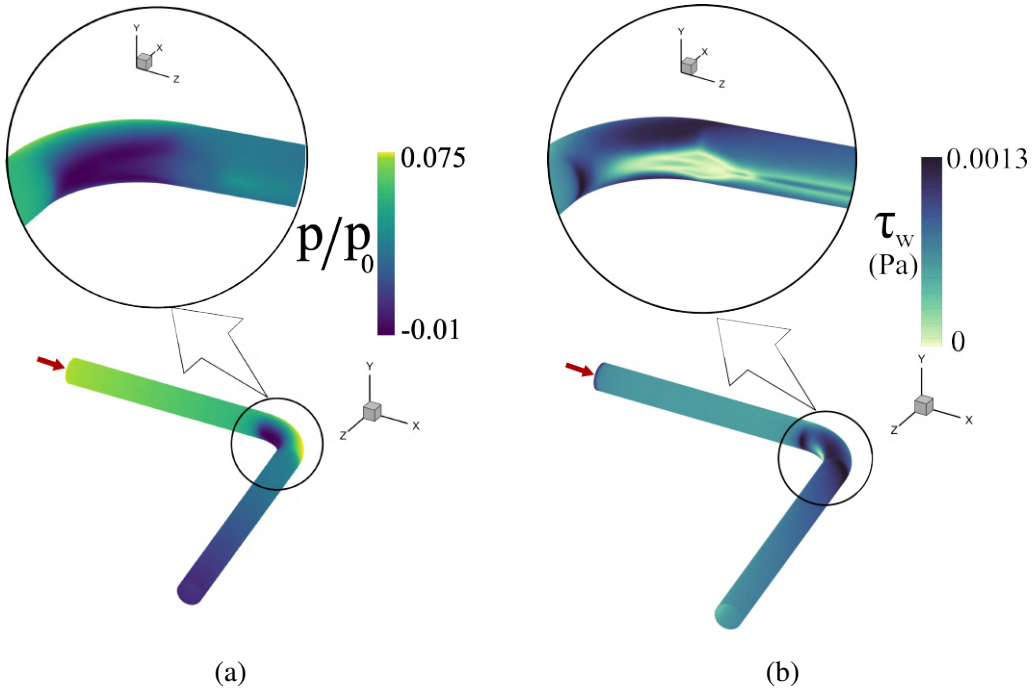

(a) (b)

Figure 4: Distribution of (a) p/p_o and (b) τ_w for the pipe bend with $\theta_b = 80°$.

is concentrated around the bend region. It is also apparent in Figure 5(b), that the maximum σ_{eq} occur in the upstream area of the pipe near the inlet. These observations consistent with the fixed displacement boundary condition applied at both ends of the pipe. The large flow induced forces ahead of the bend outlet (see Figure 4) result in a larger reaction force on the region near the pipe inlet, which thus contributes to a higher σ_{eq} noted in Figure 5(b). With increasing θ_b (results not shown here for brevity), the magnitudes of $\boldsymbol{D}$ and σ_{eq} decrease in the bend and entrance region of the pipe, respectively. A plausible reasoning can be associated with the increase in velocity deficit region, which results in a reduction of cumulative flow-induced pressure around the region of pipe bend. This, subsequently, reduces the reaction forces around the entrance region of the pipe at higher θ_b, which results in a lower σ_{eq}. The lower reaction forces also coincide with a lesser $\boldsymbol{D}$. More investigation is currently underway to confirm these findings quantitatively for the pipe bend at varying θ_b.

4 CONCLUSIONS

This numerical study demonstrates the significant impact of θ_b on FSI phenomena in pipelines using Solids4Foam. The results indicate that increasing θ_b enhances velocity deficit region ahead of the bend, while also reducing the recovery length required for damping the re-circulation region downstream. The pressure distribution and wall shear stress depict greater non-uniformity for larger θ_b, on account of the stronger re-circulation and velocity deficit regions within, and downstream of the bend. Furthermore, for the solid pipe shell, the maximum σ_{eq} occur in the

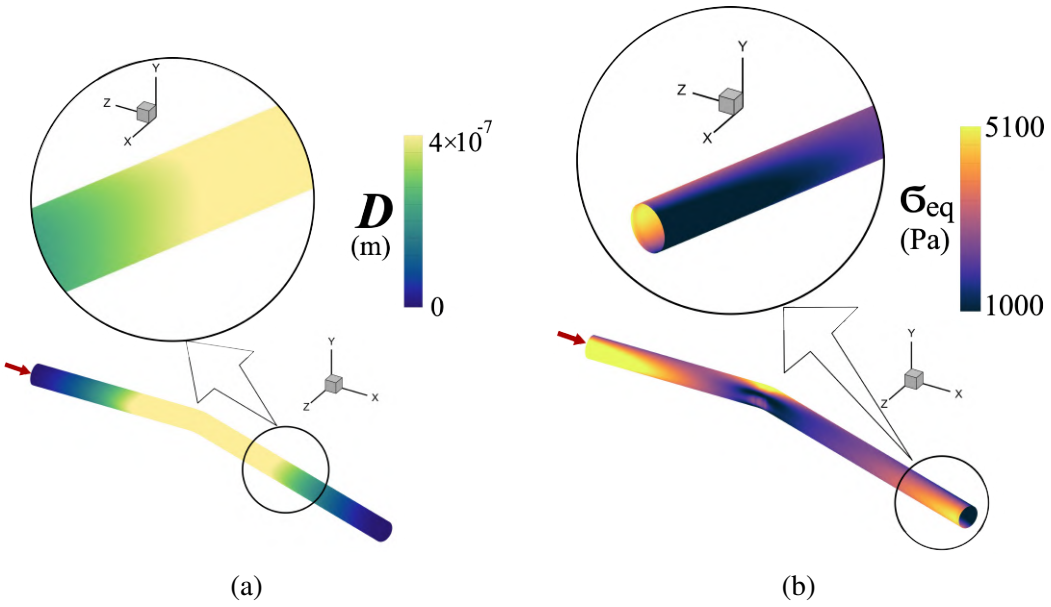

Figure 5: Distribution of (a) $\boldsymbol{D}$ and (b) σ_{eq} on the outer shell for the pipe bend with $\theta_b = 20°$.

upstream area of the bends near the inlet on account of the reaction forces imposed by the flow behavior. $\boldsymbol{D}$ in the outer shell of the pipe also decrease with increasing θ_b, highlighting the complex association between bend geometry and structural response.

By providing comprehensive insights into the behavior of FSI in bend pipes, this research contributes towards better reliability and structural integrity in pipeline designs. Future studies could further explore different pipe bend radius, flow and structural boundary conditions, to enhance the correspondence with more physical aspects of oil transportation.

REFERENCES

[1] Chen, W., Yang, Z., Hu, G., Jing, H., & Wang, J. (2022). New Advances in Fluid–Structure Interaction. *Applied Sciences*, **12**(11), 5366.

[2] Wiggert, D. C., & Tijsseling, A. S. (2001). Fluid transients and fluid-structure interaction in flexible liquid-filled piping. *ASME. Applied Mechanics Reviews, 54*(5), 455–481.

[3] Kot, C. A., Hsieh, B. J., Youngdahl, C. K., & Valentin, R. A. (1981). Transient cavitation in fluid-structure interactions. *ASME Journal of Pressure Vessel Technology, 103*(4), 345–351.

[4] Hellström, L. H., Zlatinov, M. B., Cao, G., & Smits, A. J. (2013). Turbulent pipe flow downstream of a bend. *Journal of Fluid Mechanics, 735*, R7.

[5] Hellström, L. H., Zlatinov, M. B., Smits, A. J., & Cao, G. (2011). Turbulent pipe flow through a 90 bend. In *Seventh International Symposium on Turbulence and Shear Flow Phenomena*. Begel House Inc..

[6] Sudo, K., Sumida, M., & Hibara, H. (1998). Experimental investigation on turbulent flow in a circular-sectioned 90-degree bend. *Experiments in Fluids*, 25(1), 42-49.

[7] Sudo, K., Sumida, M., & Hibara, H. (2000). Experimental investigation on turbulent flow through a circular-sectioned 180 bend. *Experiments in Fluids*, 28(1), 51-57.

[8] Spedding, P. L., Bénard, E., & McNally, G. M. (2004). Fluid flow through 90 degree bends. *Developments in Chemical Engineering and Mineral Processing*, 12(1-2), 107-128.

[9] Vaghefi, M., Akbari, M., & Fiouz, A. R. (2016). An experimental study of mean and turbulent flow in a 180 degree sharp open channel bend: Secondary flow and bed shear stress. *KSCE Journal of Civil Engineering*, 20, 1582-1593.

[10] Yarahmadi, M. B., Bejestan, M. S., & Pagliara, S. (2020). An experimental study on the secondary flows and bed shear stress at a 90-degree mild bend with and without triangular vanes. *Journal of Hydro-environment Research*, 33, 1-9.

[11] Crawford, N., Spence, S., Simpson, A., & Cunningham, G. (2009). A numerical investigation of the flow structures and losses for turbulent flow in 90 elbow bends. *Proceedings of the Institution of Mechanical Engineers, Part E: Journal of Process Mechanical Engineering*, 223(1), 27-44.

[12] Miwa, S., Mori, M., & Hibiki, T. (2015). Two-phase flow induced vibration in piping systems. *Progress in Nuclear Energy*, 78, 270-284.

[13] Pontaza, J. P., Menon, R. G., Okeremi, A., Spritzer, J., & Widjaja, S. (2013, June). Flow-induced vibrations of high gas rate well jumpers: tees vs. bends. In *International Conference on Offshore Mechanics and Arctic Engineering* (Vol. 55416, p. V007T08A082). American Society of Mechanical Engineers.

[14] Cardiff, P. (2021). Solid mechanics and fluid–solid interaction using the Solids4foam tool box.

[15] Jasak, H. (2009). OpenFOAM: Open source CFD in research and industry. *International Journal of Naval Architecture and Ocean Engineering*, 1(2), 89-94.